



Influence of SrO content on microstructure and crystallization of glazes in the $\text{SiO}_2\text{--Al}_2\text{O}_3\text{--CaO--MgO--K}_2\text{O}$ system

Marcin Gajek¹ · Alicja Rapacz-Kmita¹ · Magdalena Leśniak¹ · Ewa Stodolak-Zych¹ · Magdalena Dudek² · Maciej Sitarz¹

Received: 25 October 2018 / Accepted: 11 March 2019 / Published online: 21 March 2019
© The Author(s) 2019

Abstract

The effect of the SrO addition on the microstructure and structure of the glazes from the $\text{SiO}_2\text{--Al}_2\text{O}_3\text{--CaO--MgO--K}_2\text{O}$ system was investigated in this study. The results were obtained by testing the ability of the frits crystallization, the stability of the crystallizing phases during the single-step fast-firing cycle depending on their chemical composition and the effect of addition of strontium oxide. Differential scanning calorimetry (DSC) curves showed that all glazes crystallized, and diopside and anorthite were mainly identified as dominant phases in the obtained glazes, while the size and amount of each depended on the amount of SrO introduced. The thermal characteristic of the frits was carried out using DSC, and crystalline phases were determined by X-ray diffractometry. The glaze microstructure was investigated by scanning electron microscopy and transmission electron microscopy. Additional information on the microstructure of frits was derived from spectroscopic studies in the mid-infrared range.

Keywords Fritted glazes · Glass · SrO · Structure · Thermal analysis

Introduction

Multi-component glasses, based on glass-forming SiO_2 , are used in numerous technological solutions. In traditional ceramics, a layer of glass combined with a ceramic substrate called glaze is used to impart aesthetic qualities as well as to protect material against spotting, soaking or adverse effects of chemicals [1–4]. Depending on the type of product to which the glaze is applied, different temperatures and firing times are used, with the firing time and temperature determining the initial composition of the glaze. In two extreme cases, these are glazes that are made on the basis of raw materials or frits. In the first case, the ceramic raw materials during the firing process melt on the ceramic product creating a glaze, which occurs, for

example, in the technology of sanitary products or porcelain [4–6]. In the second case, frits are used, i.e. raw materials pre-melted into glass, and then ground, therefore during the firing process are melted faster and at a lower temperature than the raw materials from which they were produced [7]. Ceramic frits are used in the technology of ceramic tiles production, which during the fast-firing processes not exceeding several dozen minutes, melt on the ceramic product creating a continuous, flawless glaze layer. Depending on the frits used, coming from different glass systems, glazes with different properties are obtained. The final properties of glazes result from their oxide composition of frits and raw materials, the firing process carried out and the microstructure of the glazes [8]. A good example of glazes with extremely different final parameters, which depend on the chemical composition and the firing process, are transparent glazes and glass-crystalline glazes. Transparent glazes are usually characterized by a high degree of gloss [9] and create a glassy, almost completely amorphous coating. Glass-crystalline glazes may, however, be characterized by: higher mechanical resistance, degree of opacity [10], lower gloss.

✉ Alicja Rapacz-Kmita
kmita@agh.edu.pl

¹ Faculty of Materials Science and Ceramics, AGH University of Science and Technology, al. Mickiewicza 30, 30-059 Kraków, Poland

² Faculty of Energy and Fuels, AGH University of Science and Technology, al. Mickiewicza 30, 30-059 Kraków, Poland

The literature provides the results of research on various glass systems, such as MgO–Al₂O₃–SiO₂ [11–14], CaO–MgO–Al₂O₃–SiO₂ [7, 11, 15–19], Li₂O–CaO–MgO–Al₂O₃–SiO₂ [17, 20, 21], ZnO–CaO–MgO–B₂O₃–Al₂O₃–SiO₂ [22], (Na₂O, K₂O, ZrO₂, ZnO)–CaO–MgO–Al₂O₃–SiO₂ [11, 15, 17, 23–27], which can form the basis for the development of frit compositions, and consequently glazes.

The role SrO plays in glaze depends on the system it is used for, and in the structure of glass it acts as a modifier. Strontium oxide is used in glazes as a flux with a stronger effect than CaO. For glazes, it is usually introduced through frits, and its content in frits is variable and depending on the purpose may vary within the limits of 1.0–16 mass% [2]. Strontium oxide introduced into glazes instead of ZnO can, for example, inhibit the crystallization of ZrSiO₄ and allows to obtain stable, transparent glazes with a high content of ZrO₂ [5]. In other glasses [28], SrO while substituting CaO, promotes a higher content of crystalline phases. In glasses with a high SrO content, up to 25 mass%, in the presence of TiO₂ up to 4 mass%, designed for use in solid oxide cells (SOFCs) systems, glass-crystalline materials with an expansion coefficient in the range of 10.8–13.9 (10⁻⁶ K⁻¹) were obtained in which Sr₂SiO₄, Sr(TiO₃), Ca₂SiO₄ and CaSiO₃ were identified [29]. In the next work, glass-crystalline material was obtained in the BaO/SrO–MgO–B₂O₃–SiO₂ system at SrO content of 40.4 mass%, in which the crystalline phases Sr₂MgSi₂O₇ and SrB₂Si₂O₈ were present [30]. There are a number of works regarding glasses with SrO for applications in various areas [31–37]; however, its high content in these glass systems, the purpose and time of work at the target conditions, create some limitations in the possibilities of their application as a material for frits and ultimately glazes.

The main goal of this study was to investigate the effect of SrO on the structure, microstructure and crystallization of the glaze in the SiO₂–Al₂O₃–CaO–MgO–K₂O system.

Experimental

Materials and methods

The batches of components for frits from the SiO₂–Al₂O₃–CaO–MgO–K₂O system modified by the addition of SrO were prepared based on commercially available ingredients: SiO₂, Al₂O₃, CaO, MgO, K₂CO₃, SrCO₃. The chemical compositions of the studied frits are shown in Table 1.

The homogenized glaze sets in the amount of 150 g each were melted in platinum crucibles closed with a lid. Each batch was melted at 1400 °C with hold time of at the maximum temperature of 2 h, and then, the melt was rapidly cooled by pouring onto a steel plate.

Table 1 Chemical composition of the investigated frits/mass%

	SiO ₂	Al ₂ O ₃	CaO	MgO	K ₂ O	SrO
GI-0	48.27	18.93	19.25	9.55	4.00	0
GI-1	47.78	18.74	19.06	9.45	3.97	1.00
GI-2	47.06	18.46	18.76	9.31	3.90	2.51
GI-3	45.82	17.97	18.26	9.06	3.80	5.09

The morphology of the obtained and ground frits was observed using a transmission electron microscope (TEM) Jeol-JEM 1011 (100 kV accelerating voltage was used). Fourier transform infrared spectroscopy (FTIR) was used to obtain information on the structure of the studied frits, and the tests were performed using a Fourier spectrometer Bruker Optics-Vertex 70V. Samples of tested frits were prepared using the tablet method in KBr. Absorption spectra were recorded in 128 scans with a resolution of 4 cm⁻¹ in the mid-infrared range from 4000 to 400 cm⁻¹. The FTIR spectra were background corrected as described by Robbinet et al. [38], and the curves were fitted with Gaussian functions using Fityk 0.9.8. A correlation coefficient of 0.999 was obtained for all the spectra decomposition. The thermal activity of tested frits was determined by means differential scanning calorimetry (DSC) using a STA 449 F3 Jupiter (Netzsch). Frit samples (grain size below 63 μm) were heated in platinum crucibles from ambient temperature to 1220 °C at a constant rate of 10 °C min⁻¹; then, the measurement was continued by cooling the system to 600 °C. The measurement was carried out on 50 mg samples with air flow of 40 mL min⁻¹.

The aqueous suspensions of glazes, with a density of 1.6 g cm⁻³, were prepared from the ground frits (< 63 μm), which were then sprayed onto a ceramic substrate (gres-porcellanato) in an amount of 0.1 g cm⁻². The prepared glazes consisted of 100% frits. Samples were fired at 1220 °C in a fast-firing cycle; the total time of the process was 60 min with holding for 4 min at maximum temperature. Observations of the glaze microstructure were carried out using a scanning microscope (SEM) on cross sections after polishing. Nova NanoSEM 200 scanning electron microscope (FEI Europe) was used for observation and the EDAX analysis in microregions.

Phase analysis XRD was performed on pressed (30 MPa) tablets with dimensions: diameter 25 mm and height 1 mm. The tablets were then fired in the same manner as glazes. In addition, some pressed tablets were fired according to the firing curve and upon reaching the crystallization temperatures T_{c1} and T_{c2} the samples were taken out of the oven and rapidly quenched to freeze the system. Phase analysis was performed on the re-grounded material (< 63 μm) using an X-ray analysis with an X'Pert

Pro X-ray diffractometer manufactured by Philips (Panalytical).

In the work, the term frit was used in relation to melted glasses, which were denoted: GI-0, GI-1, GI-2, GI-3, respectively. The term glazes (as a traditional *set of ingredients* applied in the form of an aqueous suspension) in this work refers to samples prepared in 100% of melted frits.

Results and discussion

Frits, whose compositions are included in Table 1, after melting and pouring on a steel plate, were characterized by uniformity and were visually transparent. The prepared material was subjected to further tests. After grinding, the frits were observed in a TEM microscope and images are shown in Fig. 1.

TEM micrographs of powdered frits revealed their homogeneous nature. The beginning of liquation or crystallization was not observed.

Figure 2 shows the MIR spectra of the glasses in the range of 1600–400 cm^{-1} without and with the addition of strontium oxide. All presented spectra are characterized by the presence of three groups of bands located in the following ranges: 1350–950 cm^{-1} , 850–650 cm^{-1} and 500–400 cm^{-1} .

Detailed interpretation of the MIR spectra of amorphous materials is a very difficult task due to the large half-width of the bands (overlapping of bands). To facilitate interpretation, the MIR spectra were decomposed into samples containing 0, 2.51 and 5.09 mass% of strontium oxide (Figs. 3–5, Tables 2–4). After decomposition, the band layout in all spectra is similar. And so, the band at 1116/1080/1177 cm^{-1} is associated with asymmetric stretching vibrations Si=O (defects), band at 988/982/1067 cm^{-1} with asymmetric stretching vibrations Si–O (Si, Al)—silico–oxygen and alumino–silico–oxygen bridges (bridge bonds) [39–43], bands at 905/904/960 and 855/845/884 cm^{-1} with asymmetric stretching vibrations Si–O[−] and Al–O[−], respectively—broken silico– and alumino–oxygen bridges (terminal bonds) [40–45], bands at approximately 730 and 690 cm^{-1} with symmetric

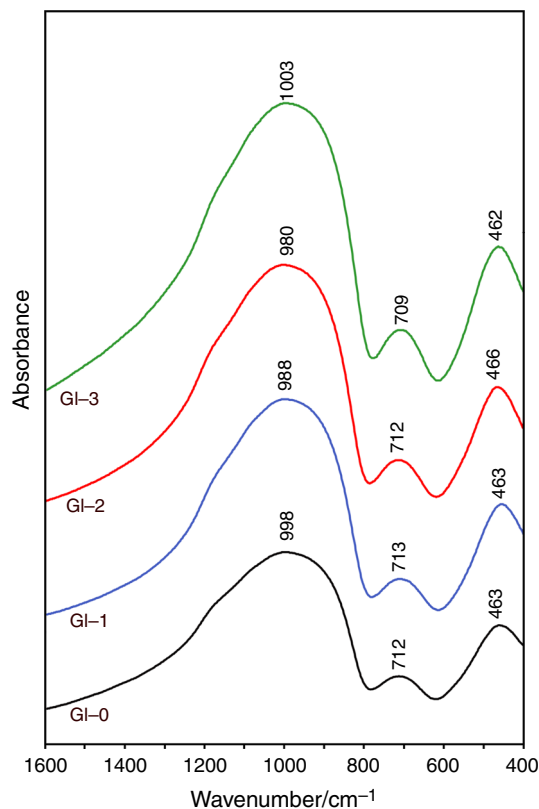


Fig. 2 FTIR spectra of glasses (frits)

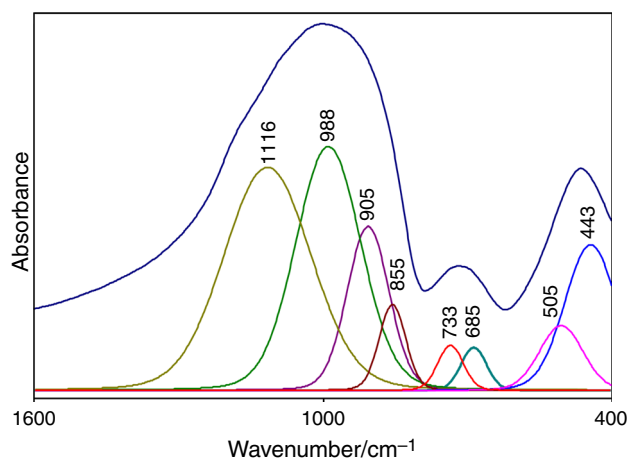


Fig. 3 Decomposition of the MIR spectrum of the GI-0 glass (0.0 mass% SrO)

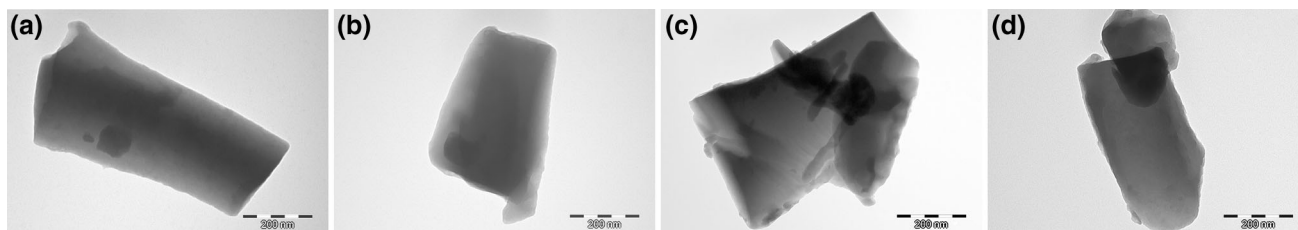


Fig. 1 The TEM images of frits: a GI-0, b GI-1, c GI-2, d GI-3

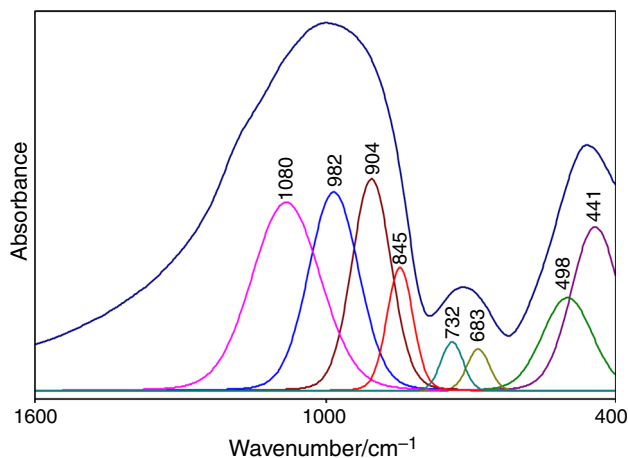


Fig. 4 Decomposition of the MIR spectrum of the Gl-2 glass (2.51 mass% SrO)

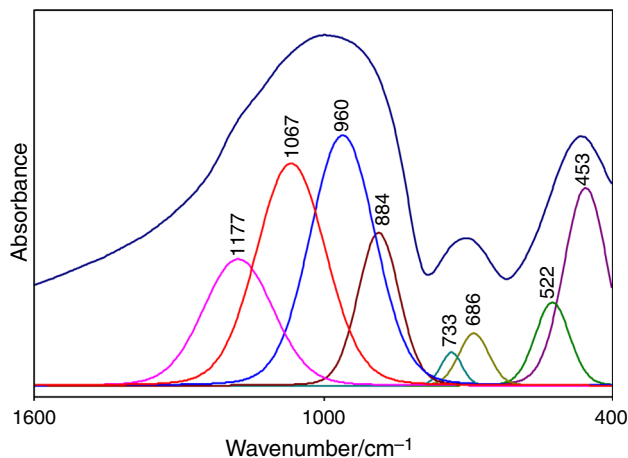


Fig. 5 Decomposition of the MIR spectrum of the Gl-3 glass (5.09 mass% SrO)

Table 2 Results of decomposition and band assignment in the MIR spectrum of Gl-0 glass (0.0 mass%)

Center	Height	Area	Assignment	$X_{0,0}$
<i>Gl-0</i>				
1116	0.25	60.76	ν_a Si = O	0.58
988	0.28	49.65	ν_a Si–O–(Si, Al)	
905	0.19	21.50	ν_a Si–O [−]	
855	0.10	7.11	ν_a Al–O [−]	
733	0.05	3.58	ν_s Si–O–Si	
685	0.04	2.56	ν_s Si–O–Al	
505	0.07	8.75	<i>R</i>	
443	0.17	23.62	δ O–(Si, Al)–O	

ν_a , asymmetric stretching vibrations; ν_s , symmetric stretching vibrations; *R*, ring vibrations; δ , bending vibrations; *X*, the ratio of the intensity of the integral band associated with the stretching vibrations Si–O (Si, Al) to the sum of the integral intensities of the bands associated with the stretching vibrations Si–O[−] and Al–O[−]

Table 3 Results of decomposition and band assignment in the MIR spectrum of Gl-2 glass (2.51 mass%)

Center	Height	Area	Assignment	$X_{2,51}$
<i>Gl-2</i>				
1080	0.18	34.60	ν_a Si=O	1.27
982	0.20	26.71	ν_a Si–O–(Si, Al)	
904	0.21	25.31	ν_a Si–O [−]	
845	0.12	8.63	ν_a Al–O [−]	
732	0.05	3.53	ν_s Si–O–Si	
683	0.04	2.53	ν_s Si–O–Al	
498	0.09	12.50	<i>R</i>	
441	0.16	21.20	δ O–(Si, Al)–O	

ν_a , asymmetric stretching vibrations; ν_s , symmetric stretching vibrations; *R*, ring vibrations; δ , bending vibrations; *X*, the ratio of the intensity of the integral band associated with the stretching vibrations Si–O (Si, Al) to the sum of the integral intensities of the bands associated with the stretching vibrations Si–O[−] and Al–O[−]

stretching vibrations Si–O–Si and Si–O–Al [26, 46, 47], bands at 505/498/522 cm^{−1} are related to vibration of aluminosilico-oxygen rings [26, 46–52], and bands at about 443/441/453 cm^{−1} to bending vibrations O–Si–O and O–Al–O (Figs. 3–5, Tables 2–4) [48–52].

To determine the effect of strontium ions on the polymerization of the aluminium–silicon network, the ratio (*X*–Tables 2–4) of the sum of the integral intensities of the bands associated with asymmetric stretching vibrations Si–O[−] and Al–O[−] to the integral intensity of the band associated with asymmetric stretching vibrations Si–O (Si, Al) was determined.

When comparing and analysing the MIR spectra of glass 0.0 mass% SrO (Gl-0) with 2.51 mass% SrO (Gl-2) (Figs. 3 and 4, Tables 2 and 3), it can be clearly stated that the main difference that should be noted is the much higher integral intensity (surface area under curve) of bands associated with terminal bonds (bands at 904 cm^{−1} and 845 cm^{−1}, Fig. 4, Table 3) and lower intrinsic intensity of the band bound to silicon and aluminium bridges (band at 982 cm^{−1}, Fig. 4, Table 3) on the Gl-2 glass spectrum with 2.51 mass% SrO with respect to the glass spectrum with 0.0 mass% SrO (Fig. 3, Table 2). The *X* ratio is much lower for glass with the addition of 2.51 mass% SrO ($X_{2,51} = 1.27$, Table 3) compared to an analogous ratio for glass without the addition of SrO ($X_{0,0} = 0.58$, Table 2). This means that the addition of strontium oxide to the initial glass composition (Gl-0) in an amount of 2.51 mass% causes depolymerization (weakening) of the aluminium–silicon network [26, 40, 44].

Also, the addition of 5.09 mass% strontium oxide increases the integral intensity of the bands originating from the broken silicon and aluminium silicon bonds

Table 4 Results of decomposition and band assignment in the MIR spectrum of Gl-3 glass (5.09 mass%)

Center	Height	Area	Assignment	$X_{5.09}$
<i>Gl-3</i>				
1177	0.10	19.94	ν_a Si=O	1.46
1067	0.18	34.75	ν_a Si–O–(Si, Al)	
960	0.21	36.64	ν_a Si–O [−]	
884	0.13	14.21	ν_a Al–O [−]	
733	0.03	1.55	ν_s Si–O–Si	
686	0.04	3.50	ν_s Si–O–Al	
522	0.07	6.46	R	
453	0.16	19.53	δ O–(Si, Al)–O	

ν_a , asymmetric stretching vibrations; ν_s , symmetric stretching vibrations; R, ring vibrations; δ bending vibrations; X, the ratio of the intensity of the integral band associated with the stretching vibrations Si–O (Si, Al) to the sum of the integral intensities of the bands associated with the stretching vibrations Si–O[−] and Al–O[−]

(bands at 960 cm^{−1} and 884 cm^{−1}, Fig. 5, Table 4) and the reduction of the intensity of the integral band derived from bridging bonds Si–O–(Si, Al) (band at 1067 cm^{−1}, Fig. 5, Table 4) with reference to glass without the addition of SrO (Fig. 3, Table 2). The value of X based on the decomposition of the MIR spectra of the Gl-3 glass (5.09 mass% SrO) is 1.46 (Fig. 5, Table 4), and similarly to the glass containing 2.51 mass% SrO it is definitely smaller with respect to the X value for glasses unmodified with strontium oxide (Fig. 3, Table 2).

Increasing the SrO content from 2.51 to 5.09 mass% leads to an increase in the X ratio. It is also worth noting that the decomposition of the MIR spectra of the glass with 5.09 mass% of SrO (Fig. 5) shows a significant shift of the

position of all bands towards higher wavenumbers with respect to the same bands in the spectral spectrum with 0.0 mass% SrO and 2.51 mass% SrO (Figs. 3 and 4, Tables 3 and 4). This indicates the stiffening of the glass network; thus in a glass containing 5.09 mass% SrO, a portion of the strontium ions breaks the bridge bonds, and the rest of them substitutes alkaline earth cations, mainly Ca²⁺ cations. It results from a similar value of the ionic radius of Sr²⁺ ions to the ionic radius of Ca²⁺ ions.

The DSC thermal analysis results of the frits investigated are shown in Fig. 6, and the summary of results is presented in Table 5. The glass transition temperature T_g of the frits tested was determined in the temperature range of 740–746 °C, and no significant differences were observed with the increase in SrO content. The high tendency to crystallize all frits was recorded on the DSC plot. Two temperature ranges were observed on the DSC curves, where exothermic effects appeared. In the first range, there are strong wide peaks (T_{c1}) with a maximum in the temperature range of 975–985 °C. In the second, the weaker exothermic peaks (T_{c2}) were recorded in the temperature range of 1203–1211 °C which appeared just after the occurrence of the endothermic melting-related effect, which for all frits occurred at the temperature of 1185 °C. In the studied frits, the maximum of crystallization peaks was observed to shift to higher temperatures with increasing SrO content. On the DSC curve of frits with 5.09 mass% SrO content, an additional two exothermic effects (T_{c3} and T_{c4}) were observed with the maximum at 1144 °C and 1113 °C, occurring during the cooling stage, demonstrating re-crystallization.

The results of conducted X-ray examinations at the crystallization temperatures T_{c1} and T_{c2} , and in the entire firing cycle for the base glaze Gl-0 and the glaze with the

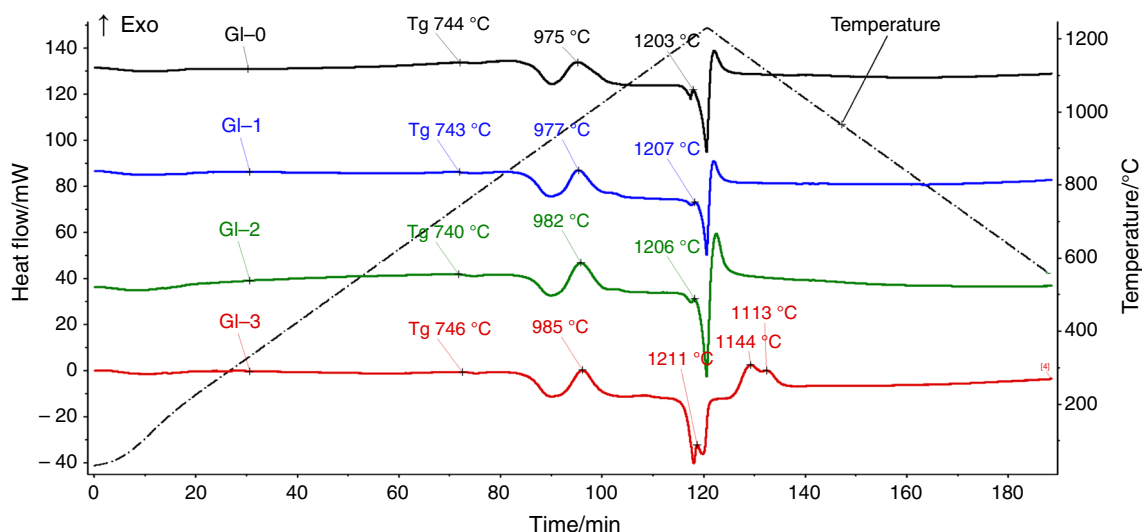
**Fig. 6** DSC curves of studied frits

Table 5 Thermal properties of frits in the SiO₂–Al₂O₃–CaO–MgO–K₂O–SrO system

Measurement technique	GI-0	GI-1	GI-2	GI-3
Transition— $T_g/^\circ\text{C}$	744	743	740	746
Crystallization effect/ $^\circ\text{C}$				
(Heating)— T_{c1}	975	977	982	985
(Heating)— T_{c2}	1203	1207	1206	1211
(Cooling)— T_{c3}	–	–	–	1144
(Cooling)— T_{c4}	–	–	–	1113

addition of 5.09 mass% SrO are shown in Figs. 7 and 8. Such a choice results from the fact that X-ray scans of GI-0, GI-1 and GI-2 glazes were almost identical. Table 6 provides a summary of the identified crystalline phases, and the estimated ratios of individual phases were determined on the basis of the intensity of individual reflections from the identified minerals.

The precise determination of the content of individual phases is due to overlapping of reflections from different phases. On the basis of X-ray images from the crystallization temperature of T_{c1} , the presence of mainly anorthite (ICSD 98-008-6328) and diopside (ICSD 98-003-3753) as well as melilite, i.e. a solid solution of akermanite/gehlenite crystalline phase (ICSD 98-016-0346), was found in glazes GI-0, GI-1 and GI-2. There was also presence of a small amount of leucite (ICSD 98-016-1635). In GI-3 glaze with 5.09 mass% SrO content, the type and number of individual phases were slightly different from other glazes.

In this glaze (GI-3), the presence of strontium feldspar [general formula $(\text{Ca}_{0.2}\text{Sr}_{0.8})(\text{Al}_2\text{Si}_2\text{O}_8)$] (ICSD 98-015-7212) and diopside as main crystalline phases was found. Larger share of akermanite/gehlenite and a lower diopside content were also observed compared to GI-0, GI-1 and GI-2 glazes. The X-ray images from the crystallization temperature T_{c2} showed the presence of the same phases as on the diffractograms registered for glazes at T_{c1} . The endothermic effect noted on the DSC curves (Fig. 6) associated with the melting of crystalline phases, which started at 1185 $^\circ\text{C}$, did not affect the total melting of the phases present in the system, but could only affect the melting of the newly crystallizing phase at T_{c2} temperature. The observed exothermic effect of T_{c2} may also result from the re-crystallization of the phases identified at the T_{c1} temperature. In addition, XRD diffractograms of GI-0, GI-1 and GI-2 glazes showed much stronger reflexes from the diopside phase. In the case of GI-3 glaze, stronger reflexes from akermanite/gehlenite were also noted. The diffractograms of samples from the entire cycle showed the presence of anorthite, diopside and leucite for glazes with contents up to 2.51 mass% SrO, and strontium feldspar, diopside and leucite for GI-3 glazes with 5.09 mass% SrO content. An increase in the intensity of reflections from diopside and the almost complete disappearance of structures from akermanite/gehlenite were also observed in all glazes. This may indicate the complete conversion to the anorthite structure according to the reaction [53, 54]:

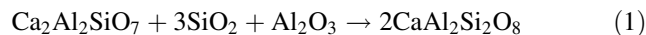
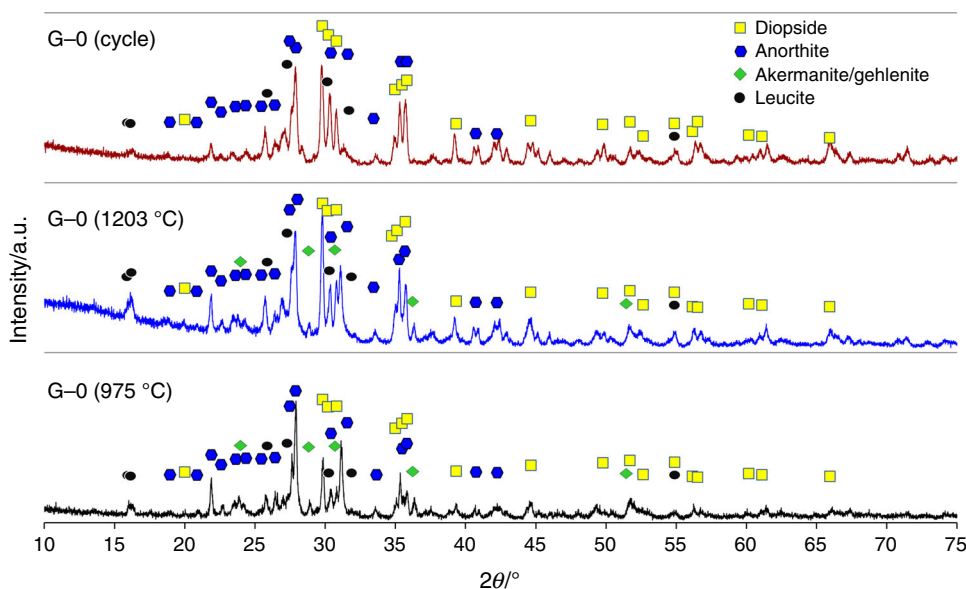
**Fig. 7** X-ray diffraction patterns of frit/glaze GI-0

Fig. 8 X-ray diffraction patterns of frit/glaze Gl-3

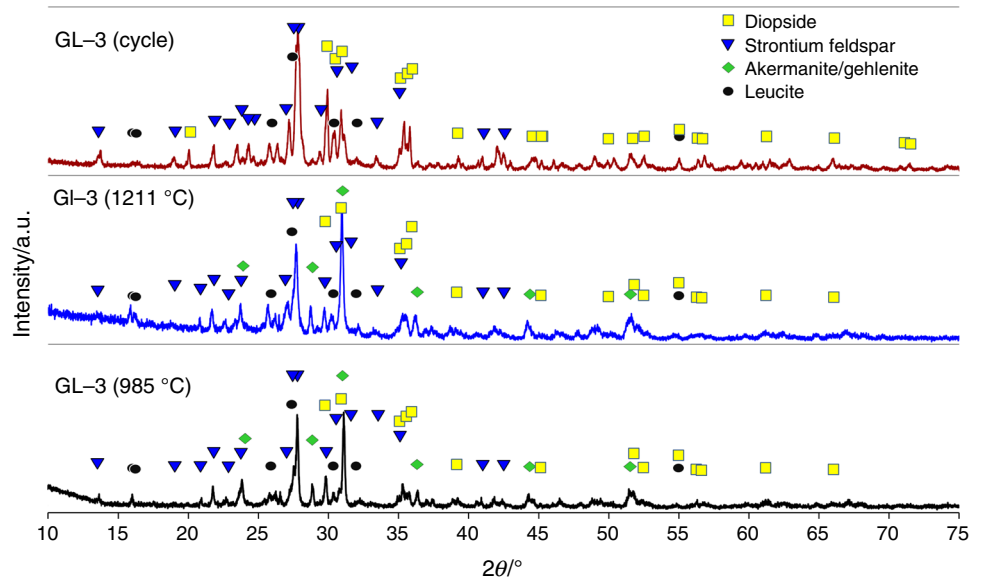


Table 6 Relative amounts of crystalline phases of tested glazes

	Gl-0		Gl-1		Gl-2		Gl-3	
$T_{c1}/^{\circ}\text{C}$	A/G	(++)	A/G	(++)	A/G	(++)	A/G	(++)
	D	(++)	D	(++)	D	(++)	D	(+)
	An	(++)	An	(++)	An	(++)	SF	(++)
	L	(+)	L	(+)	L	(+)	L	(+)
$T_{c2}/^{\circ}\text{C}$	A/G	(+)	A/G	(+)	A/G	(+)	A/G	(++)
	D	(++)	D	(++)	D	(++)	D	(+)
	An	(++)	An	(++)	An	(++)	SF	(++)
	L	(+)	L	(+)	L	(+)	L	(+)
Cycle	A/G	nd	A/G	nd	A/G	nd	A/G	nd
	D	(+++)	D	(+++)	D	(+++)	D	(++)
	An	(+++)	An	(+++)	An	(+++)	SF	(+++)
	L	(+)	L	(+)	L	(+)	L	(+)

+++ , ++ and + denotes strong, medium and weak diffraction peaks, respectively
 nd, not determined; A/G, $\text{Ca}_2(\text{Al}_{0.25}\text{Mg}_{0.75})(\text{Al}_{0.25}\text{Si}_{1.75}\text{O}_7)$ – akermanite/gehlenite; D, $\text{Ca}_{0.8}\text{Mg}_{1.2}\text{O}_6\text{Si}_2$ – diopside; An, $\text{Ca}(\text{Al}_2\text{Si}_2\text{O}_8)$ – anorthite; SF, $(\text{Ca}_{0.2}\text{Sr}_{0.8})(\text{Al}_2\text{Si}_2\text{O}_8)$ – strontium feldspar; L, $\text{K}(\text{AlSi}_2\text{O}_6)$ – leucite

Microscopic observations of the obtained glazes showed their high degree of crystallization, which is shown in Fig. 7.

Based on the SEM photos, it can be concluded that the introduction of SrO into the system caused the crystallization of a bigger amount of crystalline phase. In the Gl-0, Gl-1 and Gl-2 glazes, the shape of crystals is columnar and partially isometric, which can be clearly seen in glaze Gl-2 in which the grains of the crystalline phase are more clearly visible. The glaze with 5.09 mass% SrO content is characterized by a different morphology. In this glaze, grains of columnar and tabular shapes were observed. The conducted EDS point analysis did not show significant

differences in chemical compositions of individual phases. The crystal size is slightly higher than in glazes with a lower SrO content. These changes are related to the crystallization/formation of strontium feldspar, which is not observed in the Gl-0, Gl-1 and Gl-2 glazes, and the occurrence of crystallization at the cooling stage at temperatures T_{c3} and T_{c4} . The occurrence of crystallization in the Gl-3 glaze did not contribute to the formation of new crystalline phases (phase analysis from the whole cycle), so it can be assumed that there was a re-crystallization or the growth of already identified crystals in the system (Fig. 9).

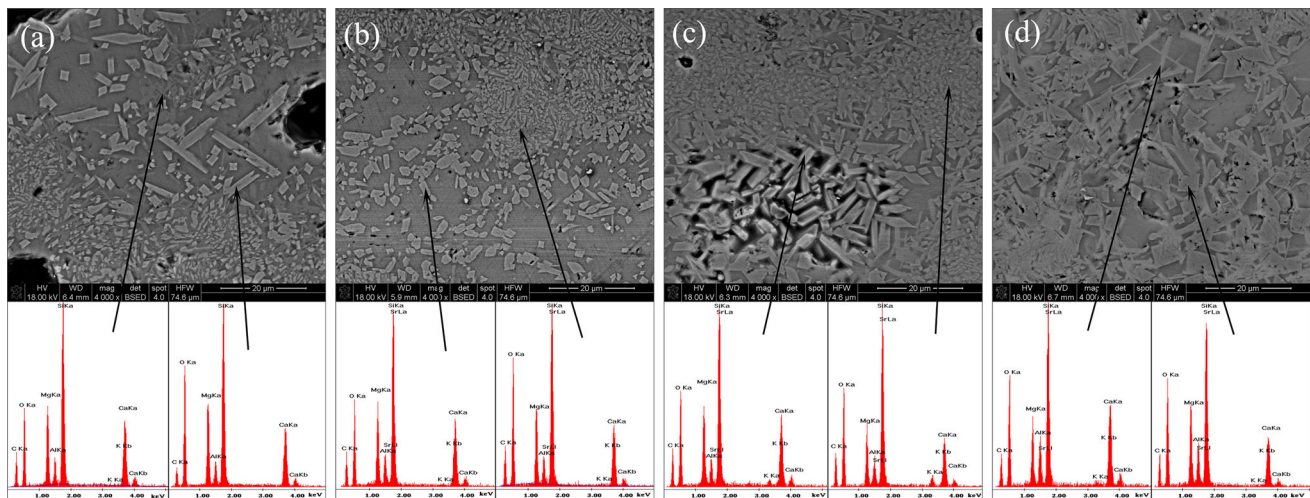


Fig. 9 SEM micrographs and EDS analysis of investigated glazes: **a** GI-0, **b** GI-1, **c** GI-2, **d** GI-3

Conclusions

The study investigated the influence of SrO content on microstructure and crystallization of glazes in the $\text{SiO}_2\text{--Al}_2\text{O}_3\text{--CaO--MgO--K}_2\text{O}$ system.

Detailed XRD and FTIR studies of frits from the $\text{SiO}_2\text{--Al}_2\text{O}_3\text{--CaO--MgO--K}_2\text{O}$ system modified with the addition of SrO allowed determination of the influence of strontium ions on their structure and microstructure. It was found that all frits are fully amorphous after melting, containing no crystalline phase and liquation. Spectroscopic studies allowed to state that at selected contents of strontium oxide, strontium ions occur in the structure of studied frits as modifying ions that depolymerize the glass network. This leads to a significant relaxation of the frit structure resulting from an increase in the number of Si--O^- bonds broken at the expense of the Si--O (Si) and Si--O (Al).

In glazes obtained from frits containing up to 2.51 mass% SrO, mainly anorthite, diopside and akermanite/gehlenite were identified. In the glaze with 5.09 mass% of SrO, feldspar strontium $[(\text{Ca}_{0.2}\text{Sr}_{0.8})(\text{Al}_2\text{Si}_2\text{O}_8)]$, diopside, akermanite/gehlenite and leucite were identified. Akermanite/gehlenite that was identified during the firing process reacted to give anorthite and was finally not observed in any glazes after firing. The introduction of SrO in the amount of 5.09 mass% also caused a change in the morphology of the obtained glaze; larger crystallites were observed, with a tabular and columnar habit compared to glazes with a lower SrO content. The increase in the content of strontium oxide in frits compositions increased the amount of crystalline phase in the fired glazes.

Acknowledgements This study was performed within the framework of funding for statutory activities of AGH University of Science and Technology in Cracow, Faculty of Materials Science and Ceramics (11.11.160.617).

Open Access This article is distributed under the terms of the Creative Commons Attribution 4.0 International License (<http://creativecommons.org/licenses/by/4.0/>), which permits unrestricted use, distribution, and reproduction in any medium, provided you give appropriate credit to the original author(s) and the source, provide a link to the Creative Commons license, and indicate if changes were made.

References

1. Stefanov S, Batscharov S. *Keramik Glasuren—ceramic glazes*. Wiesbaden: Bauverlag GmbH; 1988.
2. Epller RA, Obstler M. *Understanding glazes*. Westerville: The American Ceramic Society; 2005.
3. Epller RA, Epller DA. *Glazes and glass coatings*. Westerville: The American Ceramic Society; 2000.
4. Fortuna D. *Sanitaryware, ceramic technology*. Faenza: Gruppo Editoriale; 2000.
5. Voevodin VI. Unfitted opaque glaze for ceramic sanitary ware. *Glass Ceram*. 2000;57:250–1.
6. Gajek M, Partyka M, Rapacz-Kmita A, Gasek K. Development of anorthite based white porcelain glaze without ZrSiO_4 content. *Ceram Int*. 2017;43:1703–9.
7. Casasola R, Rincón JM, Romero M. Glass-ceramic glazes for ceramic tiles—a review. *J Mater Sci*. 2012;47:553–82.
8. Sheikhattar M, Attar H, Sharafi S, Carty WM. Influence of surface crystallinity on the surface roughness of different ceramic glazes. *Mater Charact*. 2016;118:570–4.
9. Pekkan K, Karasu B. Zircon-free frits suitable for single fast-firing opaque wall tile glazes and their industrial productions. *J Eur Ceram Soc*. 2009;29:1571–8.
10. Gajek M, Partyka M, Leśniak M, Rapacz-Kmita A, Wójcik Ł. Gahnite white colour glazes in $\text{ZnO--R}_2\text{O--RO--Al}_2\text{O}_3\text{--SiO}_2$ system. *Ceram Int*. 2018;44:15845–50.

11. Rasteiro MG, Gassman T, Santos R, Antunes E. Crystalline phase characterization of glass-ceramic glazes. *Ceram Int*. 2007;33:345–54.
12. Lira C, Novaes de Oliveira AP, Alarcon OE. Sintering and crystallisation of MgO–Al₂O₃–SiO₂ glass powders to produce cordierite glass ceramics. *Glass Technol*. 2004;45:43–8.
13. Hwang SP, Wu M. Effect of composition on microstructural development in MgO–Al₂O₃–SiO₂ glass-ceramics. *J Am Ceram Soc*. 2001;84:1108–12.
14. Gajek M, Lis J, Partyka J, Wójczyk M. Floor tile glass-ceramic glaze for improvement of the resistance to surface abrasion. In: IOP conference series: materials science and engineering, vol 18. 2011, p. 112016.
15. Torres FJ, Alarcon J. Pyroxene-based glass-ceramics as glazes for floor tiles. *J Eur Ceram Soc*. 2005;25:349–55.
16. Baldi G, Generali E, Leonelli C, Manfredini T, Pellacani GC, Siligardi C. Effects of nucleating agents on diopside crystallization in new glass-ceramics for tile-glaze application. *J Mater Sci*. 1995;30:3251–5.
17. Manfredini T. Ceramic tile glazes design, trends and applications. *Key Eng Mater*. 2002;206–213:2031–4.
18. Romero M, Rincon JM, Acosta A. Effect of iron oxide content on the crystallisation of a diopside glass–ceramic glaze. *J Eur Ceram Soc*. 2002;22:883–90.
19. Tulyaganov DU, Ribeiro MJ, Labrincha JA. Development of glass-ceramics by sintering and crystallization of fine powders of calcium–magnesium–aluminosilicate glass. *Ceram Int*. 2002;28:515–20.
20. Lisachuk GV, Shchukina LP. Phase formation processes in formation of low-melting devitrified glazes. *Glass Ceram*. 2001;58:108–10.
21. Rincón JM, Romero M, Marco J, Caballer V. Some aspects of crystallization microstructure on new glass-ceramic glazes. *Mater Res Bull*. 1998;33:1159–64.
22. Alptekin K, Kara F. Glass-ceramic glazes in the CaO–SiO₂ system. *Key Eng Mater*. 2004;264–268:1709–12.
23. Yekta BE, Alizadeh P, Rezazadeh L. Floor tile glass-ceramic glaze for improvement of glaze surface properties. *J Eur Ceram Soc*. 2006;26:3809–12.
24. Yekta BE, Alizadeh P, Rezazadeh L. Synthesis of glass-ceramic glazes in the ZnO–Al₂O₃–SiO₂–ZrO₂ system. *J Eur Ceram Soc*. 2007;27:2311–5.
25. Leśniak M, Gajek M, Partyka J, Sitarz M. Structure and thermal properties of the fritted glazes in SiO₂–Al₂O₃–CaO–MgO–Na₂O–K₂O–ZnO system. *J Therm Anal Calorim*. 2017;130:165–76.
26. Leśniak M, Gajek M, Partyka J, Sitarz M. Thermal characterisation of raw aluminosilicate glazes in SiO₂–Al₂O₃–CaO–K₂O–Na₂O–ZnO system with variable content of ZnO. *J Therm Anal Calorim*. 2017;128:1343–51.
27. Gasek K, Partyka J, Gajek M, Panna W. Characteristic of synthesis and transformations of hardystonite in willemite glass-crystalline glaze based on thermal analysis. *J Therm Anal Calorim*. 2016;125:1135–42.
28. Chang M-W, Lyoo SH, Choo HS, Lee JM. Properties of glasses based on the CaO–MgO–SiO₂ system for low-temperature co-fired ceramic. *Ceram Int*. 2009;35:2513–5.
29. Silva LD, Rodrigues AM, Rodrigues ACM, Pascual MJ, Durán A, Cabral AA. Sintering and crystallization of SrO–CaO–B₂O₃–SiO₂ glass-ceramics with different TiO₂ contents. *J Non Cryst Solids*. 2017;473:33–40.
30. Rodríguez-López S, Wei J, Laurenti KC, Mathias I, Justo VM, Serbena FC, Baudín C, Malzbender J, Pascual MJ. Mechanical properties of solid oxide fuel cell glass-ceramic sealants in the system BaO/SrO–MgO–B₂O₃–SiO₂. *J Eur Ceram Soc*. 2017;37:3579–94.
31. Reis ST, Pascual MJ, Brow RK, Ray CS, Zhang T. Crystallization and processing of SOFC sealing glasses. *J Non Cryst Solids*. 2010;356:3009–12.
32. Beall GH. Refractory glass-ceramics based on alkaline earth aluminosilicates. *J Eur Ceram Soc*. 2009;29:1211–9.
33. Chen X, Tang Y, Bo X, Song J, Luo J. Microstructures and energy storage properties of Sr_{0.5}Ba_{0.5}Nb₂O₆ ceramics with SrO–B₂O₃–SiO₂ glass addition. *J Mater Sci: Mater Electron*. 2018;29:17563–70.
34. Kim EA, Choi HW, Yang YS. Effects of Al₂O₃ on (1–x)[SrO–SiO₂–B₂O₃]_{1–x}Al₂O₃ glass sealant for intermediate temperature solid oxide fuel cell. *Ceram Int*. 2015;41:14621–6.
35. Sung Y-M, Park JS. Sintering and crystallization of (SrO–SiO₂)–(SrO–Al₂O₃–2SiO₂) glass-ceramics. *J Mater Sci*. 1999;34:5803–9.
36. Kadyrova ZR, Tuganova SK, Eminov AA. High-temperature interaction between calcium and strontium titanodisilicates. *Glass Ceram*. 2012;68:413–5.
37. Karasu B, Cable M. The chemical durability of SrO–MgO–ZrO₂–SiO₂ glasses in strongly alkaline environments. *J Eur Ceram Soc*. 2000;20:2499–508.
38. Robinet L, Bouquillon A, Hartwig J. Correlations between Raman parameters and elemental composition in lead and lead alkali silicate glasses. *J Raman Spectrosc*. 2008;39:618–26.
39. Partyka J, Leśniak M. Raman and infrared spectroscopy study on structure and microstructure of glass-ceramic materials from SiO₂–Al₂O₃–Na₂O–K₂O–CaO system modified by variable molar ratio of SiO₂/Al₂O₃. *Spectrochim Acta, Part A*. 2016;152:82–91.
40. Leśniak M, Partyka J, Sitarz M. Impact of ZnO on the structure of aluminosilicate glazes. *J Mol Struct*. 2016;1126:251–8.
41. Gritco A, Moldovan M, Grecu R, Simon V. Thermal and infrared analyses of aluminosilicate glass systems for dental implants. *J Optoelectron Adv Mater*. 2005;7:2845–7.
42. Wang F, Stamboulis A, Holland D, Matsuya S, Takeuchi A. Solid state MAS-NMR and FTIR study of barium containing aluminosilicate glasses. *Key Eng Mater*. 2008;361–363:825–8.
43. Sitarz M, Rokita M, Handke M, Galuskin EW. Structural studies of the NaCaPO₄–SiO₂ sol–gel derived materials. *J Mol Struct*. 2003;651–653:489–98.
44. Kucharczyk S, Sitarz M, Zajac M, Deja J. The effect of CaO/SiO₂ molar ratio of CaO–Al₂O₃–SiO₂ glasses on their structure and reactivity in alkali activated system. *Spectrochim Acta, Part A*. 2018;194:163–71.
45. Kaky KM, Lakshminarayana G, Baki SO, Taufiq-Yap YH, Mahdi MA. Structural, thermal, and optical analysis of zinc boro-aluminosilicate glasses containing different alkali and alkaline modifier ions. *J Non Cryst Solids*. 2017;456:55–63.
46. Aguiar H, Serra J, González P, León B. Structural study of sol-gel silicate glasses by IR and Raman spectroscopies. *Non Cryst Solids*. 2009;355:475–80.
47. Sitarz M, Handke M, Fojud Z, Jurga S. Spectroscopic studies of glassy phospho-silicate materials. *J Mol Struct*. 2005;744–747:621–6.
48. Lubas M, Sitarz M, Fojud Z, Jurga S. Structure of multicomponent SiO₂–Al₂O₃–Fe₂O₃–MgO glasses for preparation of fibrous insulating materials. *J Mol Struct*. 2005;744–747:615–9.
49. Sitarz M, Handke M, Mozgawa W, Galuskin E, Galuskin IO. The non-ring cations influence on silicoxygen rings vibrations. *J Mol Struct*. 2000;555:357–62.
50. Handke M, Sitarz M, Mozgawa W. Model of silicoxygen ring vibrations. *J Mol Struct*. 1998;450:229–38.
51. Sitarz M, Handke M, Mozgawa W. The calculations of silicoxygen rings vibrations. *Spectrochim Acta, Part A*. 1999;55:2831–7.
52. Łodziński M, Sitarz M, Stec K, Kazanecki M, Fojud Z, Jurga S. ICP, IR, Raman, NMR investigation of beryls from pegmatites of the sudety mts. *J Mol Struct*. 2005;744–747:1005–15.

53. Allu AR, Balaji S, Tulyaganov DU, Mather GC, Margit F, Pascual MJ, Siegel R, Milius W, Senker J, Agarkov DA, Kharton VV, Ferreira JMF. Understanding the formation of $\text{CaAl}_2\text{Si}_2\text{O}_8$ in melilite-based glass-ceramics: combined diffraction and spectroscopic studies. *ACS Omega*. 2017;2:6233–43.
54. Traoré K, Kabré TB, Blanchart B. Gehlenite and anorthite crystallisation from kaolinite and calcite mix. *Ceram Int*. 2003;29:377–83.

Publisher's Note Springer Nature remains neutral with regard to jurisdictional claims in published maps and institutional affiliations.